Lithos 300–301 (2018) 348–360

Contents lists available at ScienceDirect

Lithos

journal homepage: www.elsevier.com/locate/lithos

Petrogenesis of the Late Triassic diorites in the Hoh Xil area, northern Tibet: Insights into the origin of the high-Mg# andesitic signature of continental crust

Jun Wang [a,b], Guo-Ning Gou [a], Qiang Wang [a,b,c,*], Chunfu Zhang [d], Wei Dan [a,c,*], Derek A. Wyman [e], Xiu-Zheng Zhang [a]

[a] State Key Laboratory of Isotope Geochemistry, Guangzhou Institute of Geochemistry, Chinese Academy of Sciences, Guangzhou 510640, China
[b] University of Chinese Academy of Sciences, Beijing 100049, China
[c] CAS Center for Excellence in Tibetan Plateau Earth Sciences, Beijing 100101, China
[d] Department of Geosciences, Fort Hays State University, Hays, KS 67601-4099, USA
[e] School of Geosciences, The University of Sydney, NSW 2006, Australia

ARTICLE INFO

Article history:
Received 1 September 2017
Accepted 8 December 2017
Available online 12 December 2017

Keywords:
Continental crust
Fractional crystallization
High-Mg# andesites
Subduction
Tibet

ABSTRACT

An integrated petrologic, geochronologic, major and trace element geochemical, and Sr-Nd-Hf isotopic study of Late Triassic (~215 Ma) diorites from the Hoh Xil area, northern Tibet, provides new constraints on the genesis of intermediate magmas and insights into the origin of the high-Mg# andesitic signature of continental crust. These dioritic rocks are characterized by high MgO contents (3.3–5.0 wt%) and Mg# values (50–57) comparable to the estimates for the bulk continental crust at the same level of SiO_2 contents (61.1–64.5 wt%). They also display continental crust-like trace element distribution patterns and uniformly enriched isotope compositions ($[^{87}Sr/^{86}Sr]_i = 0.7081$ to 0.7094, $\varepsilon Nd[t] = -8.0$ to -6.9, and $\varepsilon Hf[t]_{zircon} = -10.1$ to -5.0). Combining our results with published data from crystallization experiments, we propose that they were probably produced by fractional crystallization from a primitive andesite parent, rather than a primitive basalt parent. This parental magma may be geochemically similar to the roughly contemporaneous primitive andesites in the adjacent Malanshan area of northern Tibet. Our compilation of modern arc lavas shows that progressive fractional crystallization of primitive andesites is also required to reproduce the Mg# versus SiO_2 array for natural arc magmas, in addition to differentiation of mantle-derived primitive basaltic magmas and/or mixing of basaltic with felsic magmas. Therefore, we emphasize that fractional crystallization of primitive andesitic magmas is potentially a frequent occurrence in arc crust and hence may play an important role in producing the high-Mg# signature of intermediate magmas comprising the continental crust.

© 2017 Elsevier B.V. All rights reserved.

1. Introduction

Continental crust is commonly considered to have andesitic to dacitic composition with SiO_2 = 57–65 wt% and Mg# = 44–55 (where Mg# = molar 100 × Mg/[Mg + Fe_{total}]) (Hacker et al., 2011; Rudnick and Gao, 2003), and yet the question of when and how it formed remains the topic of considerable debate (Hawkesworth and Kemp, 2006). Most studies conclude that arc magmatism plays a central role in generating the continental crust, because andesitic lavas found in modern subduction zones, particularly high-Mg# andesites, share striking compositional similarities with the bulk continental crust (Kelemen, 1995; Rudnick, 1995). Moreover, high-Mg# andesites and their plutonic equivalents form a recognizable part of continental crust as sanukitoids in Archean cratons (Smithies and Champion, 2000). Therefore, deciphering the petrogenesis of high-Mg# andesites and their plutonic equivalents is fundamental to understanding the origin of the high-Mg# andesitic signature of continental crust (Kelemen, 1995). Here we use the terms "primitive andesites" (lavas with 54 to 65 wt% SiO_2 and Mg# > 60) and "high-Mg# andesites" (relatively evolved lavas with 54 to 65 wt% SiO_2 and Mg# from 45 to 60) as proposed by Kelemen et al. (2003). This usage reflects the convention that lavas with Mg# < 60 are considered to be differentiated products from primitive mantle-derived magmas.

Previous studies have indicated the existence of primitive andesitic as well as basaltic magmas passing from the mantle into the crust beneath arcs (Kelemen et al., 2014 and references therein), both of which reach Fe/Mg equilibrium with mantle olivine and/or pyroxene and always have Mg# > 60 (Jagoutz and Kelemen, 2015; Straub et al., 2008). The origin of primitive andesites above subduction zones has

* Corresponding authors at: State Key Laboratory of Isotope Geochemistry (SKLaBIG), Guangzhou Institute of Geochemistry (GIG), Chinese Academy of Sciences (CAS), Wushan Street, Guangzhou 510640, China.
E-mail addresses: wqiang@gig.ac.cn (Q. Wang), danwei@gig.ac.cn (W. Dan).

https://doi.org/10.1016/j.lithos.2017.12.007
0024-4937/© 2017 Elsevier B.V. All rights reserved.

been attributed to either partial melting of strongly hydrated mantle wedge peridotites (e.g., Hirose, 1997; Mitchell and Grove, 2015; Wood and Turner, 2009) or equilibration reaction of slab-derived melts with the ultramafic mantle wedge (e.g., Kelemen et al., 2003; Shimoda et al., 1998; Tatsumi, 2001). In contrast, high-Mg# andesites and continental crust have Mg#'s too low to be in equilibrium with mantle olivine and/or pyroxene. Thus, an additional intra-crustal differentiation process acting on primitive andesites or basalts is required to produce more evolved, high-Mg# andesitic magmas (e.g., Straub et al., 2008). Three viable intra-crustal differentiation processes occurring in the arc crust have been proposed to explain the genesis of high-Mg# andesitic rocks in the arcs: (1) fractional crystallization of a primitive basalt (e.g., Blatter et al., 2013; Macpherson et al., 2006); (2) fractional crystallization of a primitive andesite (Mg# > 60) (e.g., Grove et al., 2003; Kelemen et al., 2003; Müntener et al., 2001; Tatsumi et al., 2006); and (3) mixing of primitive basaltic magma with an evolved granitic magma, which can be generated by either low-degree partial melting of preexisting crust or advanced fractionation from primitive mantle-derived magmas (e.g., Streck et al., 2007). The mixing origin for high-Mg# andesites is motivated by their disequilibrium petrographic characteristics and a reported lack of intermediate melt inclusion compositions (Reubi and Blundy, 2009). Additionally, the fact that primitive andesites are not commonly found in modern subduction zones appears to weaken the importance of the second process. Here we further evaluate the validity and importance of the intra-crustal differentiation process of primitive andesites in the generation of high-Mg# andesites akin to bulk continental crust, using our case study of the Wudaoliang diorites, a review of high-temperature crystallization experiments, and whole rock chemical analyses of natural arc lavas.

The Hoh Xil–Songpan-Ganzi (HXSG) complex (Fig. 1a) in central-western China is one of the largest flysch turbiditic basins on Earth (Nie et al., 1994). These thick turbidites, deposited during the Middle-Late Triassic, are extensively intruded by Late Triassic to Early Jurassic granitoids and are interbedded with minor volumes of volcanic rocks (Fig. 1b). In this study, we report data from the Late Triassic dioritic rocks from the Hoh Xil area in the western HXSG complex, northern Tibet (Fig. 1c). The investigated diorites have major and trace element compositions that closely resemble those of bulk continental crust. In combination with published data from high-temperature crystallization experiments (e.g., Grove et al., 2003; Müntener et al., 2001; Tatsumi et al., 2006), we argue that these diorites were generated by fractional crystallization of a primitive andesite parent geochemically similar to that from the adjacent Malanshan area of northern Tibet, rather than from a primitive basalt parent. To further explore whether fractional crystallization of primitive andesites commonly occurs in arc crust, we present a compilation of >24,670 analyses of volcanic rocks younger than 200 ka from the circum-Pacific region (data from the GEOROC database), representing convergent margin (arc) magmas. We show that progressive fractional crystallization of primitive andesites is also required, in addition to differentiation of mantle-derived primitive basaltic magmas and/or mixing of basaltic with felsic magmas, to reproduce the complete Mg# versus SiO_2 array for natural arc magmas. Thus, our

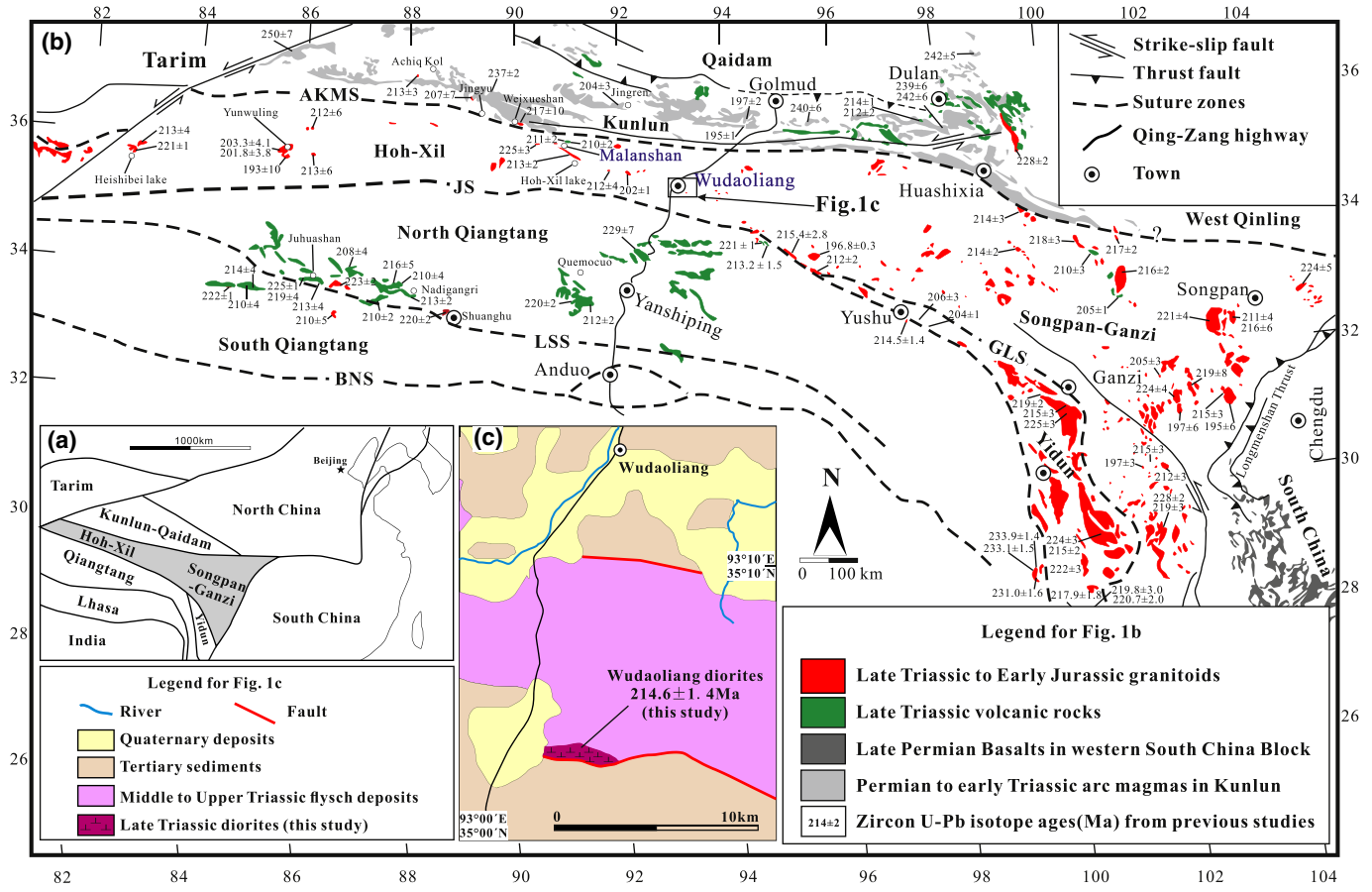

Fig. 1. (a) Tectonic sketch map of eastern Asia, with location of the Hoh Xil–Songpan-Ganzi (HXSG) complex (revised after Wang et al. (2011) and Zhang et al. (2012)). (b) Simplified tectonic map of the Tibetan Plateau showing major crustal blocks and temporal–spatial distribution of the Triassic magmatic rocks (modified from diagrams of Zhang et al. (2014) and Yin and Harrison (2000)). Ages for the Late Triassic to Early Jurassic magmatic rocks are from: Roger et al. (2004), Wang et al. (2008b, 2011), Weislogel (2008), Xiao et al. (2007), Yuan et al. (2010), Zhai et al. (2013), Zhang et al. (2006, 2007), Zhang et al. (2014) and references therein. Main suture zones between major blocks: AKMS, Anyimaqen-Kunlun-Mutztagh suture; JS, Jinshajiang suture; BNS, Bangong-Nujiang suture; GLS, Ganzi-Litang suture; LSS, Longmuco-Shuanghu suture. (c) Simplified geologic map for the Wudaoliang diorites from the Hoh Xil area in the western HXSG complex, northern Tibet.

study suggests that fractional crystallization of primitive andesitic magmas in the arc crust may have played an important role in directly forming the continental crust.

2. Geological setting and petrographical characteristics

The Tibetan Plateau is composed of a tectonic collage of different crustal blocks. From north to south, the main blocks are the Kunlun-Qaidam, Hoh Xil–Songpan-Ganzi (HXSG), Qiangtang, Lhasa, and Himalaya Blocks, separated from each other by four sutures (Anyimaqen-Kunlun-Muztagh, Jinshajiang, Bangong-Nujiang, and Yarlung-Zangbo Sutures, respectively) (Fig. 1b) (Yin and Harrison, 2000). The Qiangtang Block can be further divided into the Southern and Northern Qiangtang sub-blocks by the Longmu–Shuanghu suture (Zhang et al., 2016). The HXSG complex is a triangular-shaped orogenic belt that developed during the closure of the Paleo-Tethys Ocean basin between the North China Block (NCB) and Kunlun-Qaidam Block to the north, the South China Block (SCB) to the east, and the Qiangtang terrane and Yidun arc terrane to the south (Fig. 1b). It is characterized by the ~2.0×10^6 km^3 of Middle-Upper Triassic turbidites or flysch derived from the adjacent continental landmass (Bruguier et al., 1997; Ding et al., 2013; Nie et al., 1994). A remarkable change in sedimentary facies in the eastern HXSG complex from deep-water turbidite to terrestrial siliciclastic or tidal flat deposits (Weislogel, 2008) occurred at the end of the Norian, implying that the deepwater flysch sequence was deposited throughout most of the eastern HXSG area until the end of the Norian. Recently, Ding et al. (2013) reported Jurassic-aged detrital zircon grains in the shallow marine strata in the northwestern HXSG complex, demonstrating that marine sedimentation continued, at least locally, until the Middle Jurassic time. Thus, the closure of the Paleo-Tethys Ocean and the subsequent uplift above sea level in much of the HXSG complex may have been diachronous and younging westward.

Magmatic rocks in the HXSG complex mainly include the Late Permian basaltic rocks in the eastern margin of the HXSG complex (e.g., Song et al., 2004), Late Triassic to Early Jurassic granitoids throughout the HXSG complex (e.g., Roger et al., 2004; Xiao et al., 2007; Yuan et al., 2010; Zhang et al., 2006, 2007, 2014), and Late Triassic primitive andesites (Wang et al., 2011) in the western HXSG complex (Fig. 1b). It is worth noting that many of these granitoids (ranging in age from the Middle Triassic to latest Triassic) were intruded during ongoing deep marine sedimentation, and have a wide range of compositions, including adakitic granitoids and I-, A-, and S-type granites.

Our study area is located in the Hoh Xil area (i.e., western HXSG complex) approximately 15 km south of Wudaoliang town and close to the Qing-Zang highway (Fig. 1c). The newly discovered Wudaoliang diorite pluton intrudes into the Middle-Upper Triassic turbidites. It is gray in color, and shows medium-grained equigranular texture (Fig. 2). During field investigations, neither metasedimentary xenoliths nor mafic microgranular enclaves (MMEs) were observed within the pluton. Major rock-forming minerals of the diorites include plagioclase (~25–35 vol%), amphibole (~20–32 vol%), clinopyroxene (~5–10 vol%), biotite (~15 vol%), quartz (~10 vol%), Fe–Ti oxides (~5 vol%), and trace amounts of K-feldspar (Fig. 2). Larger plagioclases, averaging 0.2–1.0 mm in length, form subhedral to almost euhedral prisms, while relatively smaller plagioclases (60–200 μm) are subhedral to anhedral and are often enclosed by large amphibole or biotite crystals (Fig. 2a). Clinopyroxene grains are anhedral and mostly <1.0 mm in size. They are typically embedded in amphiboles (Fig. 2a). Amphibole grains are euhedral-subhedral and brown-greenish. Biotites are subhedral-anhedral and dark-brown, and anhedral biotite rims often show intergrowths with amphiboles. Fe–Ti oxides are typically

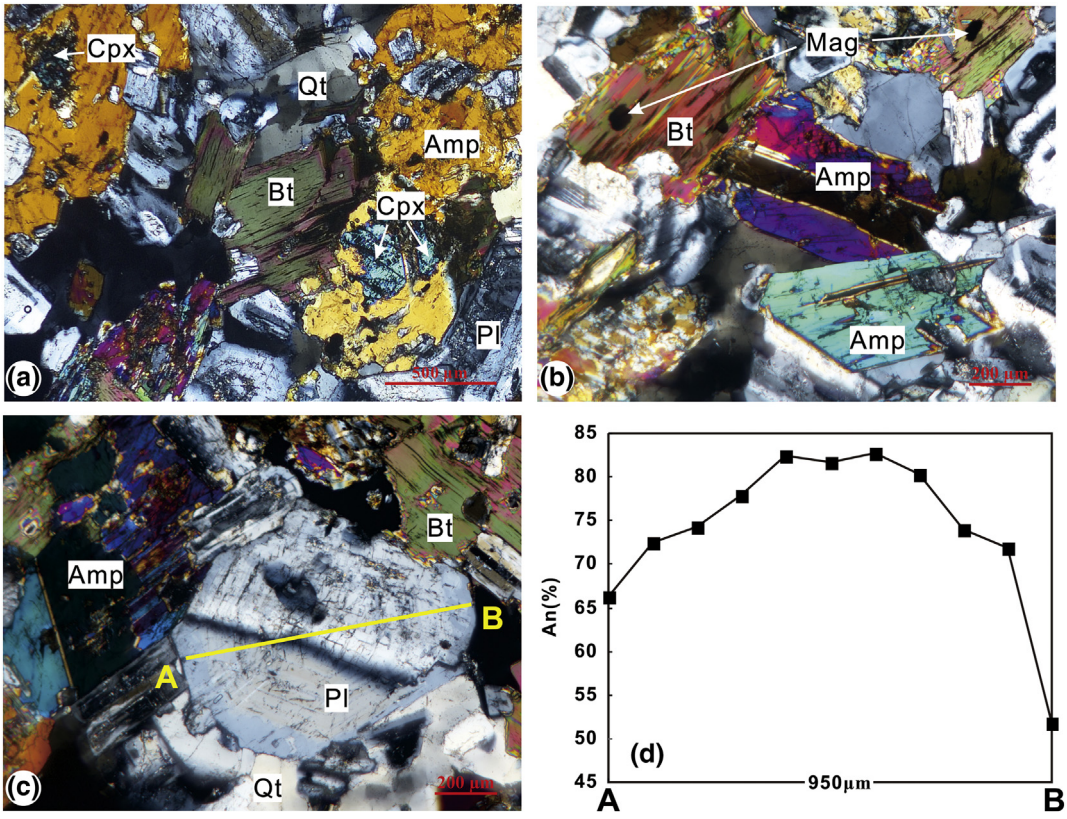

Fig. 2. (a–c) Representative photomicrographs (cross-polarized light) of the Wudaoliang diorites. (d) A geochemical traverse across the plagioclase in (c) showing variations in An (%) components. The yellow line A–B in (c) shows the location of the compositional traverse. Mineral abbreviations: Pl, plagioclase; Cpx, clinopyroxene; Amp, amphibole; Bt, biotite; Qt, quartz; Mag, titanomagnetite.

embedded in amphiboles and biotites. Quartz occurs as anhedral, interstitial crystals.

3. Results

Analytical methods are given in Appendix 1 in the Supplementary material. Also included are Laser ablation inductively coupled plasma mass spectrometry (LA-ICP-MS) zircon U-Pb geochronology data (Appendix 2); zircon Lu–Hf isotope data (Appendix 3); mineral compositions (Appendices 4–7); and major & trace elements and Sr-Nd isotope data (Appendix 8) for the Wudaoliang diorites.

3.1. Zircon U-Pb geochronology

Zircon grains from the diorite sample (10QB05-1) have a size range of 50–160 μm and length/width ratios of 1:1–3:1. CL images of the zircon grains used for LA-ICP-MS analyses show concentric compositional zoning (Fig. 3). Their high Th/U ratios (0.38–0.58) suggest a magmatic origin (Appendix 2). A total of fifteen analyses were conducted on fifteen zircon grains. Twelve of the fifteen zircons' U-Pb analyses are concordant and yield a weighted mean $^{206}Pb/^{238}U$ age of 214.6 ± 1.4 Ma (2σ) (MSWD = 0.94) (Fig. 3). This age is interpreted as the best estimate for the crystallization time of the Wudaoliang diorites. Two other analyses produce discordant ages due to significant radiogenic Pb loss, probably caused by later tectono-thermal events. The remaining one zircon grain has an older $^{207}Pb/^{206}Pb$ age of 1911 Ma. Considering that a few ca. 1600–2000 Ma detrital zircon crystals have been reported in the Triassic flysch complex (Bruguier et al., 1997), this older zircon is interpreted as a xenocryst incorporated from the wall-rocks (i.e., the Triassic flysch strata). In summary, the Wudaoliang diorites were generated in the Late Triassic, with ages similar to those obtained for the primitive andesite (ca. 210 Ma) in the northern Malanshan area of northern Tibet (Fig. 1b; Wang et al., 2011).

3.2. Mineral compositions

Clinopyroxenes are mainly diopside and augite. They exhibit relatively low Al_2O_3 (0.47–2.63 wt%) but high MgO (12.2–16.4 wt%) contents and high Mg# (66–86) (Appendix 4). All the plagioclase crystals investigated show normal zoning, with An contents ranging from 41 to 87 mol% (Appendix 6; Fig. 2c and d). Amphiboles are mainly magnesio-hornblende of the calcic-amphibole group according to the nomenclature of Leake et al. (1997), but some are slightly altered and show actinolite amphibole composition. The amphiboles have high Mg# values ranging from 62 to 83 (Appendix 5). The dark-brown micas are magnesio-biotite (Appendix 7) (Rieder et al., 1998), with high Mg# values (44–52). Fe-Ti oxides are classified as titanomagnetite or ilmenite.

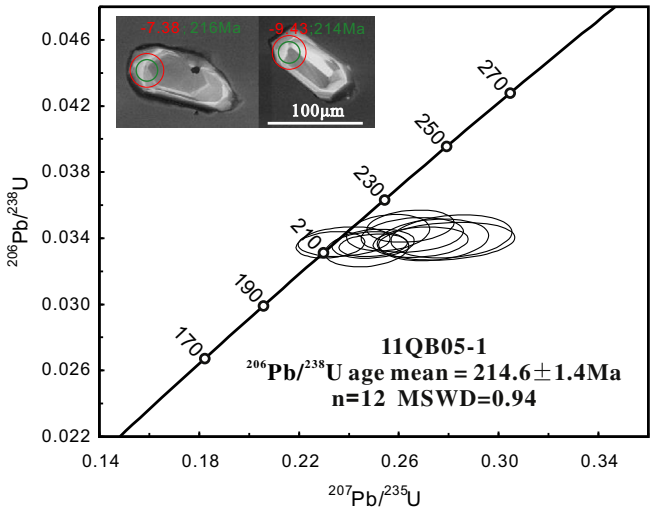

Fig. 3. LA–ICP–MS zircon U-Pb concordia diagram with representative zircon CL images for the Wudaoliang diorites. The green and red circles denote the analytical spots for U-Pb dating and Lu-Hf isotopes, respectively. The corresponding green and red numbers represent $^{206}Pb/^{238}U$ ages and εHf(t) values, respectively.

3.3. Major and trace element compositions

The Wudaoliang diorites have SiO_2 contents ranging from 61.1 to 64.5 wt% (volatile-free) (Fig. 4). Compared with all of the Late Triassic granitoids in the western HXSG complex, the Wudaoliang diorites are characterized by high MgO contents (3.3–5.0 wt%) and Mg# values (50–57), similar to estimates for the bulk continental crust at the same SiO_2 content (Fig. 4a and b). The primitive mantle-normalized trace-element distribution patterns of the Wudaoliang diorites are characterized by the enrichment of large ion lithophile elements (LILEs) and the depletion of high field strength elements (HFSEs, e.g., Nb, Ta, and Ti) (Fig. 5a). On chondrite-normalized rare earth elements (REE) diagrams, the Wudaoliang diorites show low LREE/HREE (L = Light, H = Heavy) ratios (e.g., $[La/Yb]_N$ = 4.3–7.6) (Fig. 5b) and slightly negative Eu anomalies ($Eu/Eu^* = Eu_N/SQRT[Sm_N \times Gd_N]$ = 0.71–0.79) (Figs. 5a and 7c). They also display flat HREE patterns with uniform Dy/Yb ratios ($[Dy/Yb]_N$ = 1.1–1.2) similar to those of the bulk continental crust (Fig. 5b).

The location of the approximately contemporaneous primitive andesitic lavas (ca. 210 Ma) in the northern Malanshan area, northern Hoh Xil area is shown for comparison on Fig. 1b. They are geochemically similar to Cenozoic sanukitoids in the southwestern (SW) Japan Arc (Wang et al., 2011). It should be noted that the Malanshan primitive andesites have significantly higher LOI (loss on ignition) values (4.37 to 7.34 wt%) than the Wudaoliang diorites (Appendix 8), probably due to higher degrees of alteration or low-grade metamorphism (Wang et al., 2011), which may have changed the mobile element contents of the Malanshan primitive andesites, including Ca, Na, K, and the LILEs (e.g., Rb and Cs), as well as the $(^{87}Sr/^{86}Sr)_i$ isotopic ratios. Thus, immobile elements such as Mg, Fe, Ti, transition elements (e.g., Cr and Ni), HFSEs, REEs, and Nd isotope compositions are used in the following comparison of the Wudaoliang diorites and Malanshan primitive andesites.

Compared with the Malanshan primitive andesites, the Wudaoliang diorites have relatively evolved compositions with lower MgO and higher SiO_2 contents. They have subparallel multielement variation patterns showing high Th/La but relatively low La/Yb ratios (Fig. 5), but the Malanshan primitive andesites have lower total REE contents and exhibit negligible Eu anomalies. Nonetheless, it is apparent that the trace element distribution patterns for both types of rocks are analogous to those of sanukitoids from the SW Japan Arc while also strongly resembling bulk continental crust (Fig. 5).

3.4. Sr–Nd–Hf isotope compositions

The Wudaoliang diorites have high initial $^{87}Sr/^{86}Sr$ isotopic ratios (0.7081 to 0.7094) and low εNd(t) values (−8.0 to −6.9), which overlap with those of the Late Triassic granitoids in the western HXSG complex and modern marine sediments (Fig. 6a and b). However, their Sr–Nd isotope compositions are different from those of the Late-Permian mafic rocks and Neoproterozoic igneous and metamorphic rocks in the eastern HXSG complex and western Yangtze Blocks, and Triassic flysch sediments in the western HXSG complex (Fig. 6a and b). Additionally, the εNd(t) values of the Wudaoliang diorites are slightly higher than those (−9.0 to −7.9) of the Malanshan primitive andesites (Fig. 6a and b). However, the latter is more isotopically enriched in terms of Sr, most probably due to higher degrees of alteration or low-grade metamorphism during post-magmatic processes (see previous discussion and Wang et al., 2011).

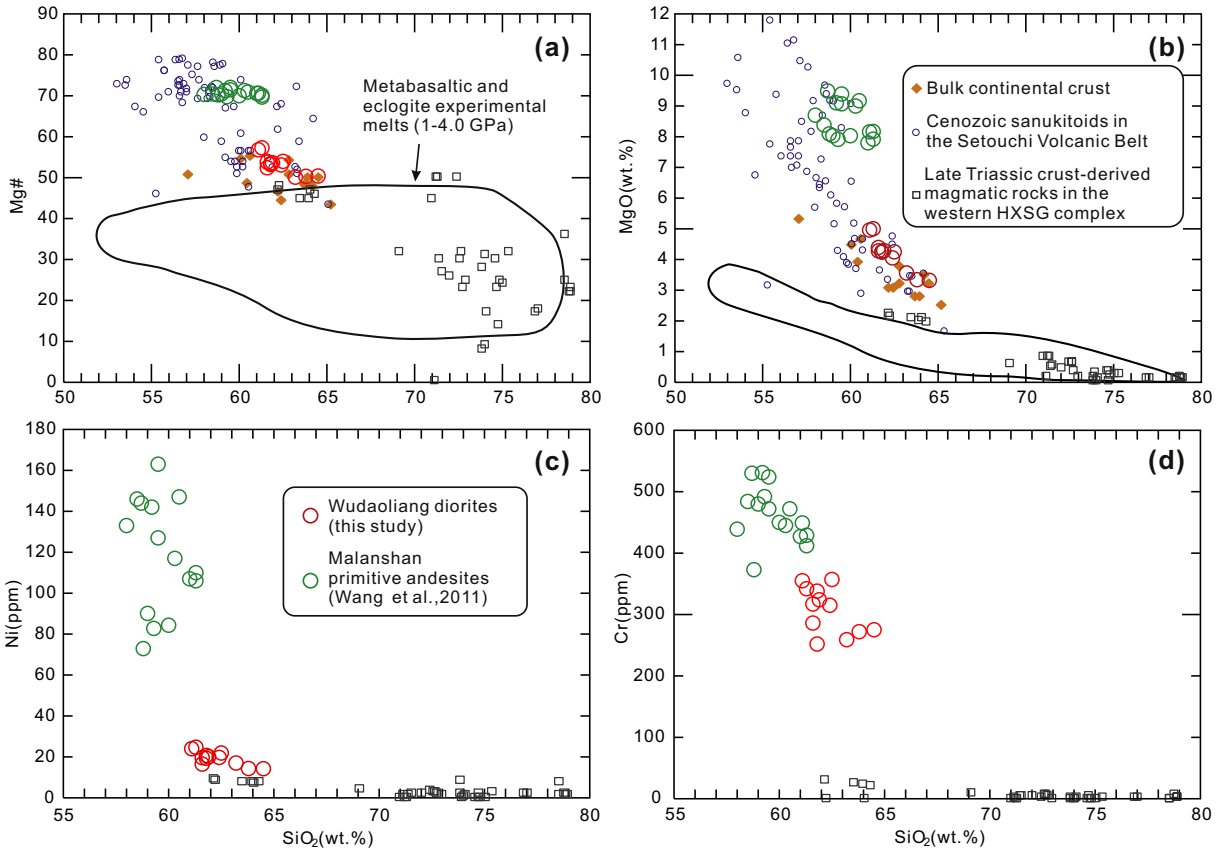

Fig. 4. (a) Mg# versus SiO_2. (b) MgO versus SiO_2. (c) Ni versus SiO_2. (d) Cr versus SiO_2. The whole-rock major element compositions have been recalculated to 100% on an anhydrous basis. The data for contemporaneous primitive andesites from the adjacent Malanshan area are shown for comparison (Wang et al., 2011). The field of metabasaltic and eclogite experimental melts (1–4.0 Ga) is from Rapp and Watson (1995) and references therein. The data for the Cenozoic sanukitoids in the Setouchi volcanic belt, Japan, are from Shimoda et al. (1998), Tatsumi (2001) and references therein. The estimates for the compositions of bulk continental crust (orange diamonds) are based on the compilations of Hacker et al. (2011) and Rudnick and Gao (2003), including 13 bulk crustal estimates. The data for the Late Triassic magmatic rocks in the western HXSG complex are from Zhang et al. (2014).

Zircon Hf isotopic analyses were conducted on the same samples that had been analyzed for U-Pb dating. Zircon Hf isotopic data from the diorite sample are illustrated in Fig. 6c and d. The magmatic zircons with ~214 Ma crystallization ages have initial $^{176}Hf/^{177}Hf$ ratios of 0.282353 to 0.282497 and εHf(t) values ranging from −10.1 to −5.0 (Fig. 6d), which are similar to those of the Late Triassic granitoids in the Hoh Xil area (Fig. 6c).

4. Discussion

4.1. Petrogenesis of the Wudaoliang diorites

4.1.1. The possibility of crustal anatexis

Intermediate to felsic magmas are often hypothesized to be formed by partial melting of mafic lower crustal rocks, which are generally

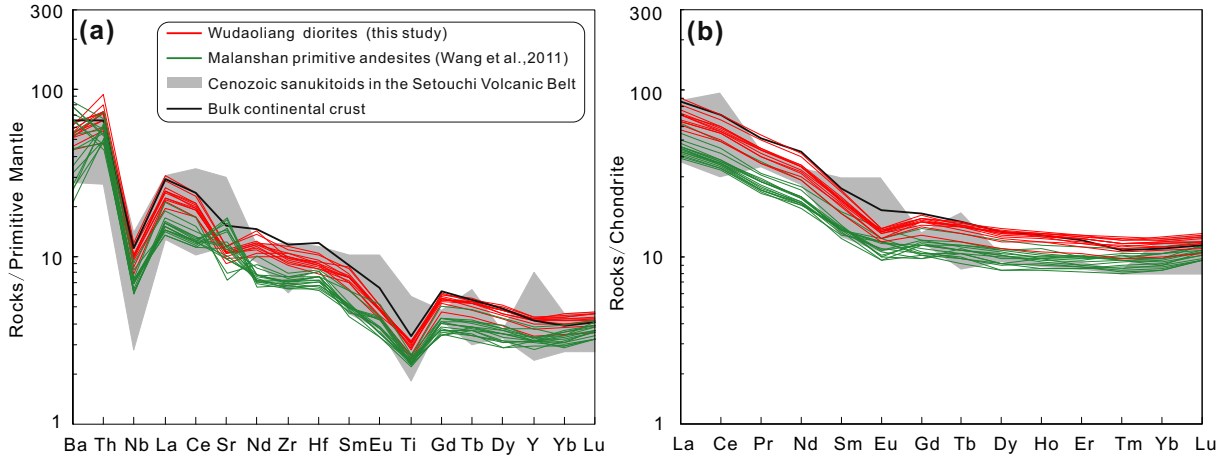

Fig. 5. Primitive mantle normalized trace element diagrams (a) and chondrite-normalized REE patterns (b) for the Wudaoliang diorites with the Malanshan primitive andesites plotted for comparison. Chondrite and primitive mantle normalized values are from Sun and McDonough (1989). The average bulk continental crust composition is from Rudnick and Gao (2003). Data sources of Cenozoic sanukitoids in the Setouchi volcanic belt are the same as in Fig. 4.

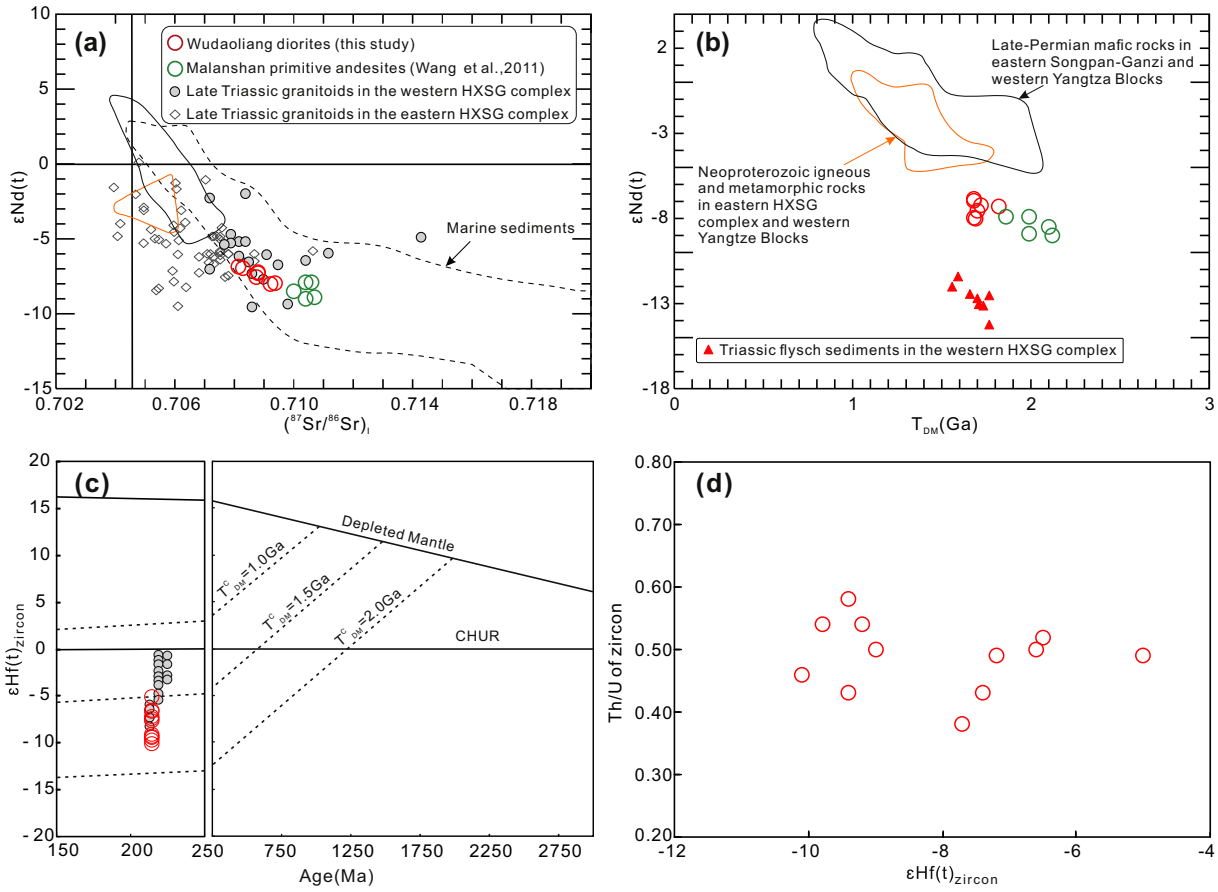

Fig. 6. Sr-Nd-Hf isotopes. (a) εNd(t) versus $(^{87}Sr/^{86}Sr)_i$. (b) εNd(t) versus T_{DM}. (c) Zircon εHf(t) values versus U–Pb ages (Ma). (d) Zircon εHf(t) values versus Th/U ratios measured for the same zircons. The data for the Late Triassic granitoids in the eastern and western HXSG complex are from the same references as in Fig. 1. The fields for the Neoproterozoic igneous and metamorphic rocks and the Late-Permian mafic rocks in the eastern HXSG complex and the western Yangtze Blocks are after Wang et al. (2008a). The data for the Triassic flysch sediments in the western HXSG complex are from Zhang et al. (2012). The data for marine sediments are from Plank and Langmuir (1998).

underplated mantle-derived magmas (e.g., Annen et al., 2006). However, the Wudaoliang diorites cannot be generated by this mechanism, because they have higher MgO contents and Mg# values than experimental melts derived from metabasalt and eclogite (1–4.0 GPa) (Fig. 4a and b) (e.g., Rapp and Watson, 1995 and references therein). In fact, all samples also have significantly higher MgO, Ni, and Cr contents than the contemporaneous crust-derived felsic rocks in the western HXSG complex (Fig. 4c and d) (Zhang et al., 2014). Moreover, some samples contain early-crystallized clinopyroxenes that have very high Cr contents (up to 2000 ppm) and Mg# (87) values (Appendix 4). The Fe-Mg exchange coefficient between Cpx and melt ($Kd^{Cpx/liquid} = [Mg^{liquid} \times Fe^{cpx}]/[Mg^{cpx} \times Fe^{liquid}]$) is only slightly dependent on temperature and has been determined to be around 0.27 ± 0.05 (Putirka, 1999). When used to calculate Mg# values, it gives results up to ~63 for the magmas in equilibrium with these clinopyroxenes. This feature also distinguishes the Wudaoliang diorite parental magmas from any purely crust-derived magmas, i.e., their parental magmas are of mantle origin. Finally, the enriched Sr-Nd isotope compositions of the Wudaoliang diorites show no affinity to the exposed basement rocks in the eastern HXSG and western Yangtze Blocks, further indicating that they were not directly derived from the partial melting of middle-lower crustal rocks (Fig. 6a and b).

4.1.2. Intra-crustal differentiation products from primitive mantle-derived magmas

While the parental magmas for the Wudaoliang diorites were of mantle origin (as stated above), they were not derived from the normal asthenosphere mantle that was isotopically depleted as recorded by normal mid-ocean ridge basalts (MORB) (Hofmann, 1988), given their continental crust-like trace element distribution patterns with enrichment of LREEs and LILEs but depletion of HFSEs and enriched Sr-Nd-Hf isotope compositions (Figs. 5 and 6). These geochemical features suggest that their parental magmas were most likely derived from an enriched mantle source metasomatized by recycled crustal materials. Alternatively, the intra-crustal differentiation processes may have incorporated crustal components into the primitive mantle-derived magmas during magma ascent and emplacement, mainly including crustal contamination and/or magma mixing of primitive magmas with crust-derived felsic magmas. Thus, determining the role of the intra-crustal differentiation processes is fundamental to understanding the petrogenesis of intermediate rocks (e.g., Reubi and Blundy, 2009; Straub et al., 2008).

Although the Wudaoliang diorite samples contain a single zircon xenocryst, their crustal contamination is considered to be insignificant for the following reasons: (1) The Wudaoliang pluton intruded into the Middle-Upper Triassic turbidites, which contain sandstones and slightly metamorphosed slates (Zhang et al., 2012), and these turbidites of the western HXSG complex have distinctly lower εNd(t) (−11.4 to −14.3) and Nb/La ratios (0.24 to 0.32) but higher SiO_2 contents (69.8 to 78.7 wt%) than the Wudaoliang diorites (Zhang et al., 2012). Thus, the products of crustal contamination should exhibit negative correlations between Nb/La and SiO_2, and positive correlations between εNd(t) and Nb/La. However, the Wudaoliang diorites show a nearly horizontal trend on a plot of Nb/La versus SiO_2 (Fig. 7b), but a weakly negative correlation on a εNd(t) versus Nb/La plot (Fig. 7a); and (2) The analyzed samples have relatively homogeneous whole-rock Nd isotopic compositions (εNd[t] = −8.0 to −6.9) (Fig. 6a), contrary to what is expected from crustal assimilation, which would generally yield variable

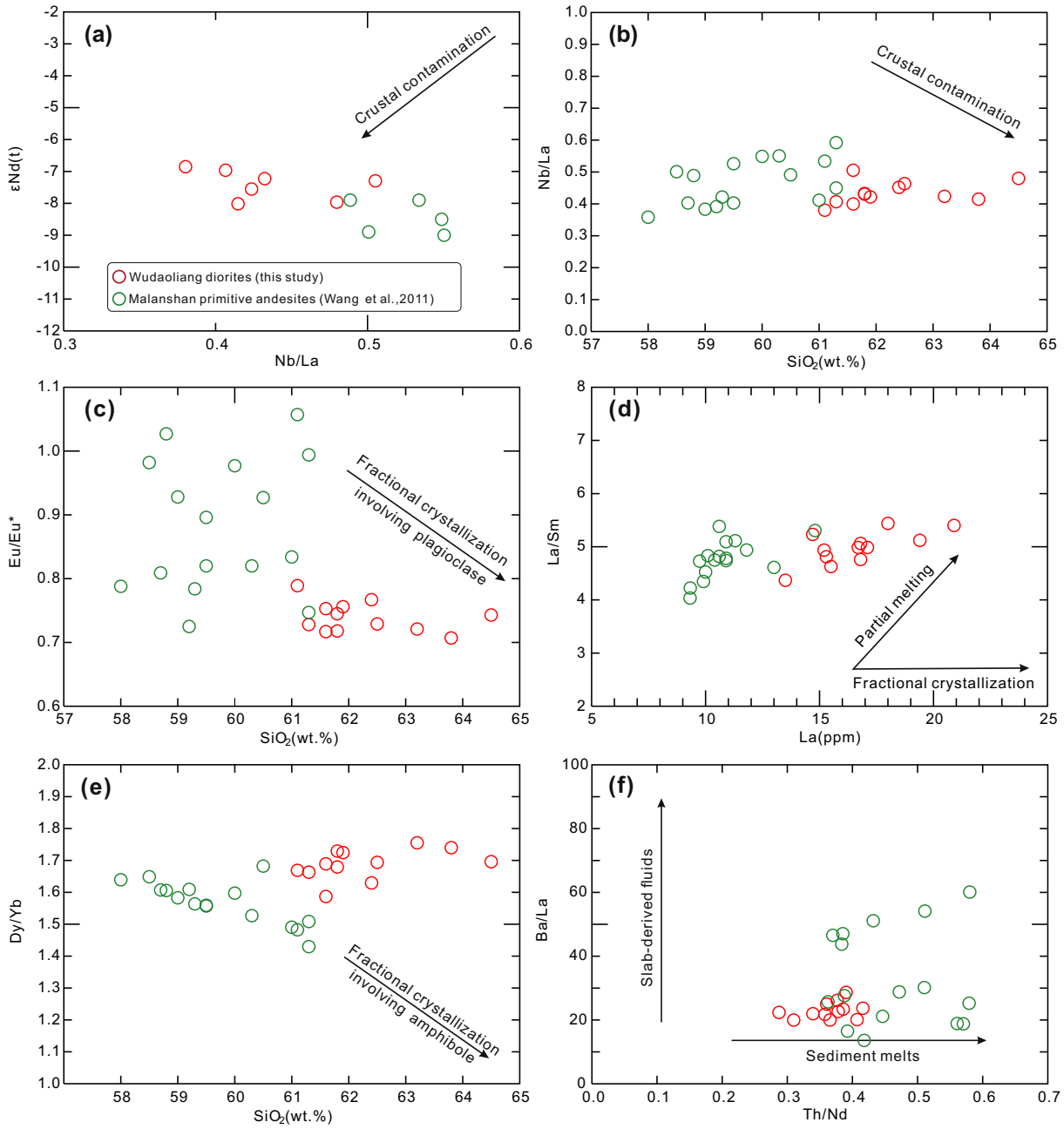

Fig. 7. (a) εNd(t) versus Nb/La. (b) Nb/La versus SiO_2. (c) Eu/Eu* versus SiO_2. (d) La/Sm versus La. (e) Dy/Yb versus SiO_2. (f) Ba/La versus Th/Nd. The trend of fractional crystallization involving amphibole in (f) is after Davidson et al. (2007). The thin arrows labeled "slab-derived fluids" and "sediment melts" in (g) indicate the trends of compositional changes due to the addition of slab-derived fluids and that of sediment melts, respectively. Symbols are as in Fig. 4.

Nd isotopic compositions. Kemp et al. (2007) proposed that a decrease in the $\varepsilon Hf(t)_{zircon}$ with decreasing Th/U ratios of zircons reflects the progressive addition of an unradiogenic crustal component to a magma chamber. Thus, the nearly horizontal trend between $\varepsilon Hf(t)_{zircon}$ and Th/U suggests that the Hf isotopic variation (−10.1 to −5.0) in zircons does not result from crustal contamination (Fig. 6d), but from source heterogeneity, because zircon grains are more capable of recording small heterogeneities than whole rocks.

Magma mixing of primitive mantle-derived magmas with crust-derived felsic magmas also cannot account for the genesis of the Wudaoliang diorites. First, magma-mixing processes is commonly accompanied by oscillatory or reverse zoning of early crystallizing phases such as plagioclase (e.g., Janoušek et al., 2004); however, the plagioclases only display simple normal zoning (Fig. 2d). Second, as discussed below, the Wudaoliang diorites show curved chemical trends on a plot of TiO_2 versus SiO_2 with a peak in TiO_2 concentration (Fig. 8b) immediately before the onset of the fractionation of Ti-bearing minerals. This trend contrasts with the linear chemical trends in element-element space produced by physical magma mixing between two compositional endmembers. In addition, no MMEs had been discovered in the Wudaoliang pluton, implying that magma mixing is unlikely to have played an important role in the genesis of the Wudaoliang diorites.

In summary, the parental magmas for the Wudaoliang diorites were insignificantly influenced by crustal contamination during magma ascent and emplacement. Thus, the crustal components evident in their geochemical characteristics must have been present in the mantle source. Considering the tectonic framework of the Late Triassic subduction of the Paleo-Tethys Ocean beneath the western HXSG complex (see discussion in Section 4.2) (Liu and Xia, 2015; Zhang et al., 2014), we suggest that such a mantle source was generated in a sub-arc mantle

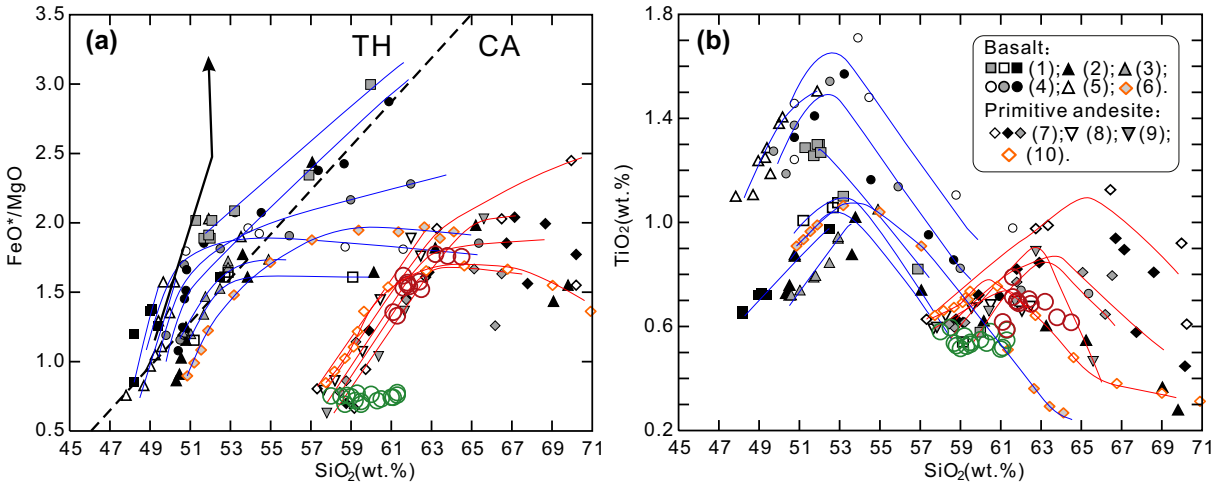

Fig. 8. Comparison of chemical variation in the quenched experimental melts and the Wudaoliang diorites (normalized anhydrous), projected on the FeO*/MgO (a) and TiO_2 (b) versus SiO_2 diagrams. The near vertical, black arrow in (a) shows the tholeiitic differentiation trend followed by anhydrous basaltic melts from Juster et al. (1989). The red and blue lines illustrate the experimental liquid lines of descent (LLD) followed by primitive andesitic melts and basaltic melts, respectively, as they experience crystal fractionation over a range of crustal pressure and at a variety of oxygen fugacities or H_2O contents. Note that the LLD obtained for primitive andesitic melts can reproduce the chemical variation trends observed for the Wudaoliang diorites. Data sources and experimental conditions: (1) Sisson and Grove (1993)—high-alumina basalt, 2 kbar, H_2O-saturated, NNO; (2) Nandedkar et al. (2014)—primitive olivine-tholeiite dike, 7 kbar, 3–10 wt% H_2O, ~NNO; (3) Hamada and Fujii (2008)—primitive basalt, 2 kbar, 1.6 wt% H_2O, NNO + 1; (4) Blatter et al. (2013)—primitive basalt, 4–9 kbar, 2 wt% H_2O, NNO + 2; (5) Pichavant and Macdonald (2007)—primitive basalt, 4 kbar, 1.6–7.7 wt% H_2O, ~NNO–NNO + 2; (6) average primitive arc basalts, 2 kbar, 2 wt% H_2O, NNO (data from the rhyolite–MELTS output); (7) Tatsumi et al. (2006)—primitive andesite, 3 kbar, 0.7–2.1 wt% H_2O, ~NNO + 3; (8) Müntener et al. (2001)—primitive andesite, 12 kbar, 5 wt% H_2O; and (9) Grove et al. (2003)—primitive andesite, 2 kbar, H_2O-saturated, NNO; (10) average primitive arc andesites, 2 kbar, 3 wt% H_2O, NNO (data from the rhyolite–MELTS output). The data for globally average primitive arc basalts and andesites are from Kelemen et al. (2014). The tholeiitic (TH)–calc-alkaline (CA) dividing line in (a) is from Miyashiro (1974).

wedge modified by subducted sediment-derived hydrous melts, mainly based on the following evidence. Mantle-derived arc magmas with distinctly enriched Hf isotope compositions generally imply a sub-arc mantle wedge enriched by subducted sediment-derived silicate melts (e.g., Woodhead et al., 2001), given that HFSEs (e.g., Hf) are insoluble in aqueous fluids but relatively mobile in silicate melts. This scenario may be applicable to the Wudaoliang samples with markedly negative zircon εHf(t) values (Fig. 6c–d). Similarly, enrichments in fluid-immobile Th relative to LREE (e.g., Th/Nd) as well as Nd isotope compositions are attributed to a partial melting of subducted sediment (Johnson and Plank, 1999; Kelemen et al., 2003). Thus, the high Th/Nd ratios of the Wudaoliang diorites indicate the presence of subducted sediment-derived partial melts in the mantle source (Fig. 7f). Moreover, the Wudaoliang diorites have REE and trace element distribution patterns showing high Th/La but relatively low La/Yb ratios, similar to the Cenozoic sanukitoids in the SW Japan Arc (Fig. 5), which are considered to have been generated by the interaction of subducted oceanic sediment-derived melts and mantle peridotites (Shimoda et al., 1998; Tatsumi, 2001).

Most or all primitive arc magmas passing from the mantle into the arc crust are in Fe/Mg exchange equilibrium with mantle olivine (Jagoutz and Kelemen, 2015), and hence a primitive mantle-derived magma should have high Mg# (>70) values (Wilson, 1989). While slab-derived melts may consume olivine in the mantle wedge and produce orthopyroxene, the primitive arc magmas in equilibrium with olivine-poor pyroxenites would still have high melt Mg# (>60) (e.g., Straub et al., 2008). In contrast, the Wudaoliang diorites have average Mg# of 53, similar to that of the bulk continental crust, which is too low to be in equilibrium with the ultramafic mantle rocks (Kelemen, 1995). The presence of interstitial quartz grains in some samples further confirms this conclusion. As mentioned above, the calculated Mg# values of the parental magmas in equilibrium with early-stage crystallized clinopyroxenes are inferred to be up to 63, suggesting that the parental magmas of the Wudaoliang diorites could be primitive magmas in near equilibrium with ultramafic mantle rocks. Thus, intra-crustal differentiation from such parental magmas is responsible for the genesis of Wudaoliang diorites.

Considering an insignificant dilution by crustal materials during magma ascent and emplacement (see discussion above), a fractional crystallization process in a closed system is probably responsible for the chemical variations in the Wudaoliang diorites, as is further corroborated by the following observations. First, on the La/Sm versus La diagram (Fig. 7d), all the Wudaoliang diorites fall along the fractional crystallization trend, showing relatively constant La/Sm but variable La contents. Second, the Wudaoliang diorites are characterized by significant negative Eu and Sr anomalies (Fig. 5), indicating that their parental magmas may have experienced some degrees of fractional crystallization of plagioclase, supported by the large plagioclase crystals (>1 cm) (Fig. 2c). Third, the negative correlations between MgO, Cr and SiO_2 (Fig. 4b, d), combined with the relatively narrow range of Ni contents (Fig. 4c), point to pyroxene-dominated fractionation without the involvement of olivine, which controls the within-suite variation for the Wudaoliang diorites. This is also consistent with a large variation of Mg# values (66–86) of the clinopyroxenes (Appendix 4). Finally, the transition from increasing to decreasing TiO_2 with increasing SiO_2 can be explained by fractionation of Ti-bearing minerals (e.g., Ti-bearing amphiboles or Fe–Ti oxides) (Fig. 8b). The almost horizontal correlations between Dy/Yb ratios and SiO_2 contents (Fig. 7e) indicate that Fe–Ti oxides, rather than amphiboles, were responsible for the within-suite variation in TiO_2 contents.

4.1.3. Nature of the parental magma: primitive andesite or basalt?

Previous studies have indicated the existence of primitive andesitic as well as basaltic magmas passing from the mantle into the crust beneath arcs (Kelemen et al., 2014 and references therein), both of which could be candidates for the parental magmas of the Wudaoliang diorites. However, we suggest that primitive andesite is the most suitable candidate based on the good agreement between the experimental and modeled liquid lines of descent (LLD) of primitive andesites and the analyzed diorites and the mismatch between those of primitive basalts and diorites (see discussion below) (Fig. 8). The modeled LLD were obtained by using the Rhyolite-MELTS thermodynamic program, which is optimized for silica-rich, fluid-bearing magmatic systems (Gualda et al., 2012). Considering that the contents of mobile elements in the

Malanshan primitive andesites, such as Ca, Na and K, have been changed due to varying degrees of alteration, we assumed two starting compositions equivalent to the globally average primitive arc andesite and basalt compiled by Kelemen et al. (2014). The modeling was carried out at pressures of 2 kbar with bulk H_2O of 3 wt% and 2 wt% for primitive andesite and basalt, respectively, given that the former may contain more H_2O than the latter (Grove et al., 2012). The modeled LLD are comparable to those from previous experimental data (Fig. 8).

It has previously been shown that the tholeiitic trend, which is characterized by early iron enrichment and only modest increases in silica content, can be reproduced experimentally at low pressure (1 atm) and anhydrous (or low H_2O) conditions (e.g., Juster et al., 1989). Under such conditions, dry basaltic magmas differentiate dominantly via crystallization of plagioclase with reduced proportions of Fe-Mg silicates, and the oxides only appear at late stages and low temperatures. Thus, it is apparent that among tholeiitic liquid series, lavas with SiO_2 contents similar to those of the Wudaoliang diorites generally have markedly high FeO*/MgO (where FeO* is total iron as FeO) ratios (~4) but low Mg# (<30) values (Fig. 8a) (Kelemen, 1995). Therefore, anhydrous basaltic magmas cannot act as the parental magmas of the Wudaoliang diorites. In contrast, elevated concentrations of dissolved H_2O (generally >2 wt%) can promote calc-alkaline differentiation of oxidized basalts by lowering the crystallization temperatures of silicates more than those of Fe-Ti oxides, causing early iron depletion and silica enrichment of derivative liquids (e.g., Grove et al., 2003; Hamada and Fujii, 2008; Pichavant and Macdonald, 2007; Sisson and Grove, 1993). Most of the experimentally produced liquids define trajectories of FeO*/MgO versus SiO_2 extending along the tholeiitic–calc-alkaline dividing line (Fig. 8a), showing an increase in FeO*/MgO with increasing SiO_2. Consequently, very few differentiated liquids with SiO_2 contents >54 wt% have Mg# values higher than 40, in accord with the observations of Kelemen (1995). Some recent experiments (e.g., Blatter et al., 2013; Nandedkar et al., 2014), under conditions of relatively high oxygen fugacities (fO_2) (e.g., ~Ni-NiO + 2), produced evolved liquids with SiO_2 > ~53 wt% that pass from the tholeiitic–calc-alkaline dividing line to plot deep into the calc-alkaline field, exhibiting only a limited increase in FeO*/MgO with markedly increasing SiO_2 (Fig. 8a). This strongly calc-alkaline differentiation trend seems to imply that the Wudaoliang dioritic samples with high Mg# (~50) values could be produced by extreme fractional crystallization from an oxidized, hydrous basaltic parent. However, the formation of high Mg# calc-alkaline andesites by this mechanism requires earlier and more abundant crystallization of Fe-Ti oxides at relatively low SiO_2 (<~53 wt%) contents (Blatter et al., 2013), as implied by the peak in TiO_2 contents of differentiated liquids appearing at SiO_2 of ~53 wt% (Fig. 8b). This also explains why the slope of the differentiation trends of basaltic magmas on the FeO*/MgO vs. SiO_2 diagram shallows markedly at relatively low SiO_2 (<~53 wt%) contents (Fig. 8a). In contrast, for crystallization sequence in the Wudaoliang diorites, Fe–Ti oxides start to join the liquidus assemblage at higher SiO_2 (~62 wt%) contents, as evidenced by the above-mentioned inflection points of differentiation trends on the FeO*/MgO ratios and TiO_2 vs. SiO_2 diagrams appearing at SiO_2 contents of ~62 wt% (Fig. 8).

Previous workers (e.g., Grove et al., 2003; Müntener et al., 2001; Tatsumi et al., 2006) have determined the phase relations and LLD of primitive andesites from the Mt. Shasta region and the Setouchi volcanic belt in the SW Japan Arc. Their results showed that the liquid differentiation paths followed by primitive andesitic magmas were parallel to those of hydrous basaltic melts (Fig. 8a). However, the former begins at a higher value of SiO_2 and the inflection points of differentiation trends on the FeO*/MgO ratios and TiO_2 vs. SiO_2 diagrams also appear at higher SiO_2 (~62 wt%) contents (Fig. 8). Similarly, the chemical variation trends in the Wudaoliang diorites show these inflection points appearing at relatively high SiO_2 (~62 wt%) contents, possibly reflecting similar mineral phases and proportions in the crystallizing assemblage. Moreover, the peak concentrations of TiO_2 in the Wudaoliang diorites are significantly lower than those of the evolved liquids from hydrous basalts (Fig. 8b), consistent with the experimental conclusion that lower TiO_2 concentration is required for Ti-bearing oxide saturation in SiO_2-richer liquids (Ryerson and Watson, 1987). Accordingly, experimental and modeled LLD of primitive andesitic magma, rather than that of primitive basaltic magma, better reproduce the chemical variation trends observed within the Wudaoliang dioritic rocks in the FeO*/MgO and TiO_2 vs. SiO_2 diagrams (Fig. 8).

More specifically, we suggest that the Wudaoliang diorites were likely generated by fractional crystallization from a primitive andesitic parent geochemically similar to that from the adjacent Malanshan area of northern Tibet as discussed below.

(1) Geochronology studies reveal that the eruption age of the Malanshan primitive andesites is 210.4 ± 1.9 Ma (Wang et al., 2011), which is similar to the crystallization age (214.6 ± 1.4 Ma) of the Wudaoliang diorites, considering the range of analytical error, and implying a possible petrogenetic link.
(2) The Wudaoliang diorites and the Malanshan primitive andesites with lowest SiO_2 contents show geochemical differentiation trends in their major element diagrams (Fig. 8), in accord with the LLD of hydrous primitive andesites from the experimental studies. It should be noted that the within-suite compositional variation in the Malanshan primitive andesites was not mainly caused by shallow-level fractional crystallization but mantle source heterogeneity or varying degrees of partial melting. This is because the almost horizontal correlation between SiO_2 and Mg# values (Fig. 4a) cannot have resulted from fractional crystallization of mafic minerals. Thus, the parental magmas of the Wudaoliang diorites were most likely represented by the member with the lowest SiO_2 content among the Malanshan primitive andesites.
(3) The compositional trends for both types of rocks fall along the fractional crystallization trend on the La/Sm vs. La diagram (Fig. 7d). Moreover, the Malanshan primitive andesites with lowest SiO_2 contents have significantly higher Eu/Eu* ratios (Fig. 7c), MgO, Ni, and Cr contents (Fig. 4b–d) than the Wudaoliang diorites, implying that differentiation between them may have resulted from fractional crystallization of olivine, pyroxene, and plagioclase. This mineral assemblage was also found in previous experimental results (e.g., Grove et al., 2003; Tatsumi et al., 2006), possibly reflecting similar experimental conditions and starting material compositions. The experimental pressure (~2 kbar) is within the estimated crystallization pressure range (0.8 to 2.5 kbar) (Appendix 5) for the Wudaoliang dioritic rocks based on the Al-in-hornblende barometry of Schmidt (1992), which also supports this conclusion.
(4) As discussed in Section 4.1.2, the Wudaoliang diorites with high Th/La but relatively low La/Yb ratios were most likely derived from an enriched mantle source that had incorporated subducted sediment-derived melts, in coincidence with the features of mantle sources for the Malanshan primitive andesites (Wang et al., 2011). However, the mantle source of the Wudaoliang diorites probably contained a smaller subducted sediment component than that of the Malanshan primitive andesites, considering that the former has slightly higher $\varepsilon Nd(t)$ values than the latter (Fig. 6a).

4.2. Tectonic setting of the Late Triassic magmatism in the western HXSG complex

The tectonic environment and petrogenesis of the extensive Late Triassic felsic magmatic rocks in the HXSG complex remain the subjects of intense debate. Most previous studies were concentrated on the eastern part of the HXSG complex (Fig. 1b). The association of A-type granite (211 Ma) with adakitic granitoids (224–216 Ma) in the eastern HXSG

complex was thought to have resulted from Triassic lithospheric delamination after crustal thickening due to convergence between the SCB, NCB, and North Tibet continental blocks (Xiao et al., 2007; Zhang et al., 2006, 2007). Recently, based on the Triassic intrusive rocks (224–205 Ma) in the eastern HXSG complex, Yuan et al. (2010) proposed that the Songpan-Ganzi basin, in which the HXSG turbidites were deposited, was similar to a foreland basin formed in response to an arc-continental collision and the resultant flexure and fracturing of the western SCB lithosphere. The two models above imply that the basement of the eastern HXSG complex could have been a continental peninsula into the Paleo-Tethys Ocean from the SCB.

In contrast to the eastern part of the basin, the western part contains no old (e.g., Neoproterozoic) metamorphic basement rocks with South China affinity. The isotopic compositions of the Late Triassic granitoids in the western HXSG complex are also different from those of contemporaneous granitoids in the eastern HXSG complex (Fig. 6a). Moreover, the closure of the Paleo-Tethys Ocean and the subsequent continent–continent collisions may have been diachronous along strike and younged westward, as stated above. That is, the continuation of marine deposition in the western HXSG complex into the Middle Jurassic suggests that the narrow western part of the Paleo-Tethys Ocean survived until this time (Ding et al., 2013). Therefore, models developed based on the eastern HXSG studies may not have fully characterized the coeval evolution of the western HXSG complex. Recently, Wang et al. (2011) suggested that the Late Triassic primitive andesites of northern Hoh Xil were generated in a Kunlun fore-arc setting. In addition, Zhang et al. (2014) proposed that the Late Triassic granitoids in the western HXSG complex were generated by partial melting of overlying continental arc fragments which were initially rifted from the Kunlun arc due to back-arc extension. Meanwhile, deep marine gravity flow deposits that temporally overlap magmatism were accumulated in the rapidly expanding Mediterranean-style back-arc basin in response to rollback of the subducting Paleo-Tethys oceanic slab (Ding et al., 2013; Pullen et al., 2008). Thus, strong attenuation of the Kunlun continental arc crust followed by possible seafloor spreading due to back-arc extension also provides sufficient accommodation space for the vast flysch sediments, implying that coeval arc magmas may be underlain by thin continental crust or even juvenile oceanic crust (Pullen et al., 2008). According to the hypothesis proposed by Tamura et al. (2016), primitive arc andesites are commonly produced in shallow and hydrous mantle (<20 km) melting, which is consistent with data from the Izu-Ogasawara (Bonin) and Aleutian oceanic arcs. In contrast, volcanoes on thicker arc crust will tend to produce more basaltic magmas and cannot produce primitive andesites because of primitive magmas in equilibrium with mantle peridotite at higher pressures. Similarly, the lack of Late Triassic arc basaltic rocks reported in the HXSG complex and the presence of primitive andesites and their differentiated products on thin arc crust coincide with the above hypothesis. Therefore, we also suggest that the extensive Late Triassic magmatism in the western HXSG complex, including the Wudaoliang diorites, should be attributed to the northward subduction of the Paleo-Tethyan Ocean, although questions remain as to whether the development of the back-arc basin and the coeval arc magmatism were related to the northward subduction of the Anyimaqen-Kunlun-Muztagh Ocean (Zhang et al., 2014) or Jinshajiang Ocean (Liu and Xia, 2015; Zhang et al., 2008) (Fig. 1b).

4.3. Insights into the origin of the high-Mg# andesitic signature of continental crust

A long-standing theory for the genesis of continental crust is that it is formed in subduction zones because andesitic rocks (particularly high-Mg# andesites [Mg# > 45]) as well as their plutonic equivalents found in subduction-related volcanic arcs have geochemical compositions similar to the continental crust (Kelemen, 1995). As mentioned earlier, three explanations have been offered for the genesis of high-Mg# andesitic rocks in the arcs (Jagoutz and Kelemen, 2015). These include fractional crystallization of a relatively low-Si, high-Fe mineral assemblage, rich in Fe–Ti oxides and/or amphibole from primitive basalt with high H_2O content and fO_2; mixing of basaltic magma with evolved granitic magma; and/or fractional crystallization of primitive andesitic magma. Despite our results, it is still unclear whether the fractional crystallization of primitive andesitic magmas occurs commonly in the arc crust, in addition to the first and second processes. Therefore, we present a compilation of >24,670 analyses of volcanic rocks from the circum-Pacific region, representing both continental and oceanic arc magmas. The raw data in this study are primarily extracted from a global dataset of whole rock chemical analyses used in Turner and Langmuir (2015), which was obtained by carefully compiling and screening data of arc front stratovolcano samples younger than 200 ka from the GEOROC database (http://georoc.mpch-mainz.gwdg.de/georoc/). Moreover, we also show in detail the compositions of arc lavas from the well-studied Aleutian subduction zone to further support our conclusions. The main purpose is to highlight the systematics of Mg# and SiO_2 contents in the arc lavas that must be accounted for by processes occurring in the mantle source and overlying arc crust.

On the abundance density contour plot of Mg# vs. SiO_2 for >24,670 arc lavas from the circum-Pacific region, the three peaks in the abundance density contours show that the most commonly analyzed rocks have compositions of ~53 wt% SiO_2 with a Mg# of ~52, ~60 wt% SiO_2 with a Mg# of ~50, and ~61 wt% SiO_2 with a Mg# of ~41 (Fig. 9a). It is noteworthy that a number of arc lavas with SiO_2 contents >54 wt% have Mg# values higher than 50, closely resembling the bulk continental crust with the composition of high-Mg# andesite (Hacker et al., 2011; Rudnick and Gao, 2003). As mentioned above, recent experimental results (e.g., Blatter et al., 2013; Nandedkar et al., 2014) indicated that evolved andesitic liquids with high Mg# values reaching a maximum of 50 could be generated by fractionation of primitive basaltic parents with relatively high fO_2 of ~Ni-NiO + 2 buffer (Fig. 8). However, the fO_2 in those experiments probably approximates an upper bound on the fO_2 of arc magmas which is generally estimated to range from Ni-NiO to Ni-NiO + 2 buffer (Carmichael, 1991; Parkinson and Arculus, 1999). Therefore, it is difficult to generate large quantities of andesitic rocks with Mg# values higher than 50 in the dataset of arc lavas solely by fractionation of hydrous basaltic magmas, even with the highest fO_2 of arc magmas (Fig. 9a). Instead, we suggest that crystal fractionation of primitive andesites is the dominant process in generating intermediate magmas with Mg# values higher than 50, as is the case for the Wudaoliang diorites from this study. On the basis of the natural arc trend for Mg# versus SiO_2, magma mixing played only a subordinate role: (1) magma mixing between primitive basaltic magma (Mg# > 60) and evolved rhyolitic magma could produce andesites with markedly higher Mg# (>50), but this mixing process will also lead to the formation of dacitic to rhyolitic (>63 wt% SiO_2) melts with higher Mg# than natural arc lavas at a given level of SiO_2 content (Fig. 9a). This is because the Mg# values of mixed magmas are dominantly controlled by the basic endmember (i.e., primitive basalt) that has MgO and FeO contents much higher than the acid endmember. (2) Mass balance considerations require that magma mixing involves roughly equal volumes of basalt and rhyolite, followed by efficient mixing to generate high-Mg# andesites. However, our compiled dataset (Fig. 9a), as well as other published arc rock datasets (e.g., Lee and Bachmann, 2014), show that the volume of exposed rhyolites is less than that of basalts. In addition, it also remains unclear whether a magma mixing process involving roughly equal volumes of basalt and rhyolite would be efficient, because mafic magmas with higher solidus and liquidus temperatures are likely to solidify upon contact with felsic melts, decreasing the efficiency of such mixing (Sparks and Marshall, 1986). Similarly, recent studies show that the mixing of mafic enclaves into felsic host plutons may be rate-limited by chemical reactions between the enclave and host pluton (Farner et al., 2014). (3) In the Aleutian case specifically, the experimental LLD for primitive andesites and basalts replicate key features of the Mg# versus SiO_2 arc lava array. For these natural Aleutian lavas, the

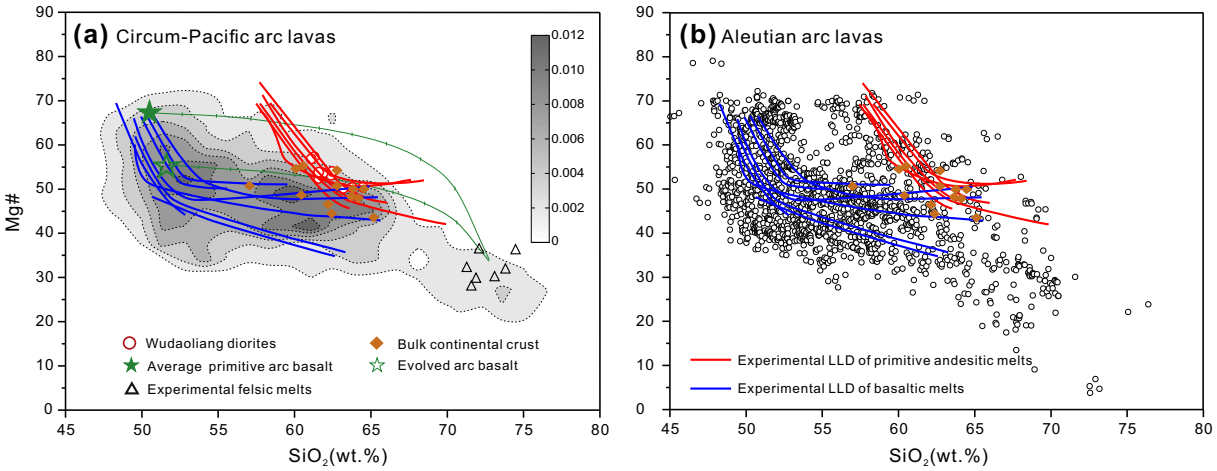

Fig. 9. (a) Abundance density contour plot of Mg# (= molar 100 × Mg/[Mg + Fe_{total}]) versus SiO_2 (wt%) for >24,670 arc lavas from the circum-Pacific region, representing both continental and oceanic arc magmas (Data from the GEOROC database). Dashed contours give the abundance density (%) of compositions plotting within each 3.6 Mg# × 1.4 wt% SiO_2 cells and hence the darker area has a higher density. For example, within the 1.2% abundance density contour, there were >296 samples within each cell, whereas within the 0.2% abundance density contour, there were only 49 samples within each cell. Note that a number of arc lavas with SiO_2 > 54 wt% have Mg# > 50, closely resembling bulk continental crust with the composition of high-Mg# andesite. Also shown for comparison are the experimental liquid lines of descent (LLD) of primitive andesitic melts (red lines) and basaltic melts (blue lines). Data sources of the experiments are the same as in Fig. 8. Two mixing curves are shown as the green lines with ticks on them that link up the end members at 10% intervals. The two corresponding mafic endmembers are represented by the average primitive arc basalt (green filled star) (Kelemen et al., 2014) and relatively evolved basalt (green open star) formed by 10% olivine crystallization from the former. The common felsic endmember is represented by the average composition of evolved experimental liquids (open triangles) with >70 wt% SiO_2 produced by Sisson et al. (2005). (b) Relationship between SiO_2 and Mg# for Aleutian arc lavas. Most of data are compiled by Kelemen et al. (2003) and the remaining data published subsequently are from the GEOROC database. Data sources of the estimates for the compositions of bulk continental crust (orange diamonds) are the same as in Fig. 4. Also shown are the data for the Wudaoliang diorites (red open circles).

SiO_2 contents of all analyzed samples with Mg# > 50 display a significant gap (Fig. 9b; see also Fig. 10 in Kelemen et al., 2003), implying that high-Mg# andesites in the Aleutian arc cannot be derived from basalts by fractional crystallization, or by progressive mixing of silicic magmas or crustal materials into mafic magmas. This is also consistent with trace-element evidence presented by Kelemen et al. (2014). Nonetheless, it should be noted that most other intermediate arc lavas with Mg# < 50 may be mainly derived from basaltic magmas by crystal fractionation (e.g., Lee and Bachmann, 2014), possibly with a secondary role for crustal contamination and/or magma mixing.

Primitive andesites may contain more H_2O than primitive basalts (Grove et al., 2012). If so, they will become H_2O saturated and degas at mid-crustal depths. As a result of degassing, these magmas will undergo rapid crystal fractionation. Thus, as shown in Fig. 9a, the paucity of primitive andesites relative to primitive basalts would also imply that most of them have already differentiated into evolved andesites and dacites, as evidenced by the relative abundance of high-Mg# andesitic arc lavas (Fig. 9a). Also, degassing together with higher SiO_2 contents of primitive andesites and their evolved products compared to basalts may lead to an increase in viscosity, implying that they may be preferentially emplaced as intrusive silicic plutonic rocks in the crust rather than being erupted (Kelemen, 1995). For the above reasons, we believe crystal fractionation of primitive andesites to be the dominant intra-crustal process for directly generating high-Mg# andesites similar to the continental crust, while both crystal fractionation from primitive basalts and magma mixing only played secondary roles. In the case of the origin of the high-Mg# andesitic signature of continental crust, an additional mechanism, such as delamination, is still required to remove the associated dense cumulates (Arndt and Goldstein, 1989; Kay and Kay, 1993; Rudnick, 1995). This process could readily change the Mg# of the crust from a value of ~70, typical for primitive melts in equilibrium with mantle olivine, to the value of ~50 estimated for the bulk continental crust.

In summary, the high-Mg# andesitic nature of continental crust can in part be explained by crystal fractionation from a primitive arc andesite composition, followed by delamination of the corresponding cumulates. Our conclusions do not rule out other mechanisms playing a certain role in generating the high-Mg# andesitic signature of continental crust, such as simple mechanical juxtaposition of unrelated solid basalts and granites. This mechanism, however, does not account for the presence of a number of high-Mg# andesitic arc lavas and mid-crustal plutons with high-Mg# andesite compositions in the tectonically exposed arc crustal section (Jagoutz and Kelemen, 2015). Considering that most of the growth of continental crust may well have occurred before or during the Archean (e.g., Dhuime et al., 2012) and that sanukitoids with high Mg# andesitic compositions form a recognizable part of the Archean rocks (Smithies and Champion, 2000), additional work is needed to assess whether primitive andesites dominate mantle-derived (primary) magmas in the early Earth (e.g., Tamura et al., 2016).

5. Conclusions

The Wudaoliang diorites from the Hoh Xil area in the western HXSG complex were emplaced in the Late Triassic (214.6 ± 1.4 Ma). The investigated diorites have major and trace element compositions that closely resemble those of the bulk continental crust. In combination with published data on high-temperature crystallization experiments, we suggest that these diorites were generated by fractional crystallization of olivine, pyroxene, and plagioclase, with minor Fe-Ti oxides from a primitive andesitic parent geochemically similar to that from the adjacent Malanshan area of northern Tibet, rather than a primitive basaltic parent. Furthermore, we present a compilation of >24,670 analyses of volcanic rocks younger than 200 ka from the circum-Pacific region, representing convergent margin (arc) magmas. The Mg# versus SiO_2 array for natural arc magmas shows that fractional crystallization of primitive andesites commonly occurs in the arc crust. Thus, we emphasize that fractional crystallization of primitive andesitic magmas in the arc crust may have played an important role in producing the high-Mg# signature of intermediate magmas comprising the continental crust.

Acknowledgements

We are very grateful for constructive comments by two anonymous reviewers and editorial handling by Prof. Xian-Hua Li. We appreciate

the assistance of Xi-Rong Liang, Xiang-Lin Tu, Jin-Long Ma, Guang-Qian Hu and Ying Liu for zircon age and geochemical analyses. We also thank Xiaoyu Fang, Li-Peng He and Jia Guo for their helpful suggestions and discussion. Financial support for this research was provided by the National Key R & D Program of China (2016YFC0600407), the Key Program of the Chinese Academy of Sciences (QYZDJ–SSW–DQC026), the National Natural Science Foundation of China (grant nos. 41630208 and 41573027), the Talent Project of Guangdong Province (2014TX01Z079), and the Guangzhou Institute of Geochemistry, Chinese Academy of Sciences (GIGCAS 135 Project [135TP201601]). This is contribution No. IS-2484 from GIGCAS.

Appendix A. Supplementary data

Supplementary data to this article can be found online at https://doi.org/10.1016/j.lithos.2017.12.007.

References

Annen, C., Blundy, J., Sparks, R., 2006. The genesis of intermediate and silicic magmas in deep crustal hot zones. Journal of Petrology 47, 505–539.

Arndt, N.T., Goldstein, S.L., 1989. An open boundary between lower continental crust and mantle: its role in crust formation and crustal recycling. Tectonophysics 161, 201–212.

Blatter, D.L., Sisson, T.W., Hankins, W.B., 2013. Crystallization of oxidized, moderately hydrous arc basalt at mid-to lower-crustal pressures: implications for andesite genesis. Contributions to Mineralogy and Petrology 166, 861–886.

Bruguier, O., Lancelot, J.R., Malavieille, J., 1997. U–Pb dating on single detrital zircon grains from the Triassic Songpan–Ganze flysch (Central China): provenance and tectonic correlations. Earth and Planetary Science Letters 152, 217–231.

Carmichael, I.S., 1991. The redox states of basic and silicic magmas: a reflection of their source regions? Contributions to Mineralogy and Petrology 106, 129–141.

Davidson, J., Turner, S., Handley, H., Macpherson, C., Dosseto, A., 2007. Amphibole "sponge" in arc crust? Geology 35, 787–790.

Dhuime, B., Hawkesworth, C.J., Cawood, P.A., Storey, C.D., 2012. A change in the geodynamics of continental growth 3 billion years ago. Science 335, 1334–1336.

Ding, L., Yang, D., Cai, F.L., Pullen, A., Kapp, P., Gehrels, G.E., Zhang, L.Y., Zhang, Q.H., Lai, Q.Z., Yue, Y.H., Shi, R.D., 2013. Provenance analysis of the Mesozoic Hoh-Xil-Songpan-Ganzi turbidites in northern Tibet: implications for the tectonic evolution of the eastern Paleo-Tethys Ocean. Tectonics 32, 34–48.

Farner, M.J., Lee, C.-T.A., Putirka, K.D., 2014. Mafic–felsic magma mixing limited by reactive processes: a case study of biotite-rich rinds on mafic enclaves. Earth and Planetary Science Letters 393, 49–59.

Grove, T.L., Elkins-Tanton, L.T., Parman, S.W., Chatterjee, N., Muntener, O., Gaetani, G.A., 2003. Fractional crystallization and mantle-melting controls on calc-alkaline differentiation trends. Contributions to Mineralogy and Petrology 145, 515–533.

Grove, T.L., Till, C.B., Krawczynski, M.J., 2012. The role of H_2O in subduction zone magmatism. Annual Review of Earth and Planetary Sciences 40, 413–439.

Gualda, G.A.R., Ghiorso, M.S., Lemons, R.V., Carley, T.L., 2012. Rhyolite-MELTS: a modified calibration of MELTS optimized for silica-rich, fluid-bearing magmatic systems. Journal of Petrology 53, 875–890.

Hacker, B.R., Kelemen, P.B., Behn, M.D., 2011. Differentiation of the continental crust by relamination. Earth and Planetary Science Letters 307, 501–516.

Hamada, M., Fujii, T., 2008. Experimental constraints on the effects of pressure and H_2O on the fractional crystallization of high-Mg island arc basalt. Contributions to Mineralogy and Petrology 155, 767–790.

Hawkesworth, C.J., Kemp, A.I.S., 2006. Evolution of the continental crust. Nature 443, 811–817.

Hirose, K., 1997. Melting experiments on lherzolite KLB-1 under hydrous conditions and generation of high-magnesian andesitic melts. Geology 25, 42–44.

Hofmann, A.W., 1988. Chemical differentiation of the earth: the relationship between mantle, continental crust, and oceanic crust. Earth and Planetary Science Letters 90, 297–314.

Jagoutz, O., Kelemen, P.B., 2015. Role of arc processes in the formation of continental crust. Annual Review of Earth and Planetary Sciences 43, 363–404.

Janoušek, V., Braithwaite, C.J., Bowes, D., Gerdes, A., 2004. Magma-mixing in the genesis of Hercynian calc-alkaline granitoids: an integrated petrographic and geochemical study of the Sázava intrusion, Central Bohemian Pluton, Czech Republic. Lithos 78, 67–99.

Johnson, M.C., Plank, T., 1999. Dehydration and melting experiments constrain the fate of subducted sediments. Geochemistry, Geophysics, Geosystems 1, 1007.

Juster, T.C., Grove, T.L., Perfit, M.R., 1989. Experimental constraints on the generation of FeTi basalts, andesites, and rhyodacites at the Galapagos Spreading Center, 85 W and 95 W. Journal of Geophysical Research: Solid Earth 94, 9251–9274.

Kay, R.W., Kay, S.M., 1993. Delamination and delamination magmatism. Tectonophysics 219, 177–189.

Kelemen, P.B., 1995. Genesis of high Mg# andesites and the continental crust. Contributions to Mineralogy and Petrology 120, 1–19.

Kelemen, P.B., Yogodzinski, G.M., Scholl, D.W., 2003. Along-strike variation in the Aleutian Island Arc: genesis of high Mg# andesite and implications for continental crust, inside the subduction factory. American Geophysical Union 223–276.

Kelemen, P.B., Hanghøj, K., Greene, A.R., 2014. 4.21 - one view of the geochemistry of subduction-related magmatic arcs, with an emphasis on primitive andesite and lower crust A2. In: Holland, Heinrich D., Turekian, K.K. (Eds.), Treatise on Geochemistry, second edition Elsevier, Oxford, pp. 749–806.

Kemp, A.I., Hawkesworth, C.J., Foster, G.L., Paterson, B.A., Woodhead, J.D., Hergt, J.M., Gray, C.M., Whitehouse, M.J., 2007. Magmatic and crustal differentiation history of granitic rocks from Hf-O isotopes in zircon. Science 315, 980.

Leake, B.E., Woolley, A.R., Arps, C.E., Birch, W.D., Gilbert, M.C., Grice, J.D., Hawthorne, F.C., Kato, A., Kisch, H.J., Krivovichev, V.G., 1997. Nomenclature of amphiboles: report of the subcommittee on amphiboles of the international mineralogical association commission on new minerals and mineral names. American Mineralogist 82, 1019–1037.

Lee, C.-T.A., Bachmann, O., 2014. How important is the role of crystal fractionation in making intermediate magmas? Insights from Zr and P systematics. Earth and Planetary Science Letters 393, 266–274.

Liu, W.L., Xia, B., 2015. Age and geochemistry of western Hoh-Xil–Songpan-Ganzi granitoids, northern Tibet: implications for the Mesozoic closure of the Paleo-Tethys ocean: comment. Lithos 212–215, 453–456.

Macpherson, C.G., Dreher, S.T., Thirlwall, M.F., 2006. Adakites without slab melting: high pressure differentiation of island arc magma, Mindanao, the Philippines. Earth and Planetary Science Letters 243, 581–593.

Mitchell, A.L., Grove, T.L., 2015. Melting the hydrous, subarc mantle: the origin of primitive andesites. Contributions to Mineralogy and Petrology 170, 1–23.

Miyashiro, A., 1974. Volcanic rock series in island arcs and active continental margins. American Journal of Science 274, 321–355.

Müntener, O., Kelemen, P.B., Grove, T.L., 2001. The role of H_2O during crystallization of primitive arc magmas under uppermost mantle conditions and genesis of igneous pyroxenites: an experimental study. Contributions to Mineralogy and Petrology 141, 643–658.

Nandedkar, R.H., Ulmer, P., Müntener, O., 2014. Fractional crystallization of primitive, hydrous arc magmas: an experimental study at 0.7 GPa. Contributions to Mineralogy and Petrology 167, 396–402.

Nie, S.Y., Yin, A., Rowley, D.B., Jin, Y.G., 1994. Exhumation of the Dabie Shan ultra-high-pressure rocks and accumulation of the Songpan-Ganzi flysch sequence, central China. Geology 22, 999–1002.

Parkinson, I.J., Arculus, R.J., 1999. The redox state of subduction zones: insights from arc-peridotites. Chemical Geology 160, 409–423.

Pichavant, M., Macdonald, R., 2007. Crystallization of primitive basaltic magmas at crustal pressures and genesis of the calc-alkaline igneous suite: experimental evidence from St Vincent, Lesser Antilles arc. Contributions to Mineralogy and Petrology 154, 535–558.

Plank, T., Langmuir, C.H., 1998. The chemical composition of subducting sediment and its consequences for the crust and mantle. Chemical Geology 145, 325–394.

Pullen, A., Kapp, P., Gehrels, G.E., Vervoort, J.D., Ding, L., 2008. Triassic continental subduction in central Tibet and Mediterranean-style closure of the Paleo-Tethys Ocean. Geology 36, 351–354.

Putirka, K., 1999. Clinopyroxene-liquid equilibria to 100 kbar and 2450 K. Contributions to Mineralogy and Petrology 135, 151–163.

Rapp, R.P., Watson, E.B., 1995. Dehydration melting of metabasalt at 8–32 kbar: implications for continental growth and crust-mantle recycling. Journal of Petrology 36, 891–931.

Reubi, O., Blundy, J., 2009. A dearth of intermediate melts at subduction zone volcanoes and the petrogenesis of arc andesites. Nature 461, 1269–1273.

Rieder, M., Cavazzini, G., D'yakonov, Y.S., Frank-Kamenetskii, V.A., Gottardi, G., Guggenheim, S., Koval', P.V., Mueller, G., Neiva, A.M., Radoslovich, E.W., 1998. Nomenclature of the micas. Clays and Clay Minerals 46, 586–595.

Roger, F., Malavieille, J., Leloup, P.H., Calassou, S., Xu, Z., 2004. Timing of granite emplacement and cooling in the Songpan-Garze Fold Belt (eastern Tibetan Plateau) with tectonic implications. Journal of Asian Earth Sciences 22, 465–481.

Rudnick, R.L., 1995. Making continental crust. Nature 378, 571–577.

Rudnick, R.L., Gao, S., 2003. 3.01 - composition of the continental crust A2. In: Holland, Heinrich D., Turekian, K.K. (Eds.), Treatise on Geochemistry. Pergamon, Oxford, pp. 1–64.

Ryerson, F.J., Watson, E., 1987. Rutile saturation in magmas: implications for TiNbTa depletion in island-arc basalts. Earth and Planetary Science Letters 86, 225–239.

Schmidt, M.W., 1992. Amphibole composition in tonalite as a function of pressure: an experimental calibration of the Al-in-hornblende barometer. Contributions to Mineralogy and Petrology 110, 304–310.

Shimoda, G., Tatsumi, Y., Nohda, S., Ishizaka, K., Jahn, B.M., 1998. Setouchi high-Mg andesites revisited: geochemical evidence for melting of subducting sediments. Earth and Planetary Science Letters 160, 479–492.

Sisson, T.W., Grove, T.L., 1993. Experimental investigations of the role of H_2O in calc-alkaline differentiation and subduction zone magmatism. Contributions to Mineralogy and Petrology 113, 143–166.

Sisson, T.W., Ratajeski, K., Hankins, W.B., Glazner, A.F., 2005. Voluminous granitic magmas from common basaltic sources. Contributions to Mineralogy and Petrology 148, 635–661.

Smithies, R., Champion, D., 2000. The Archaean high-Mg diorite suite: links to tonalite–trondhjemite–granodiorite magmatism and implications for early Archaean crustal growth. Journal of Petrology 41, 1653–1671.

Song, X.Y., Zhou, M.F., Cao, Z.M., Robinson, P.T., 2004. Late Permian rifting of the South China Craton caused by the Emeishan mantle plume? Journal of the Geological Society, London 161, 773–781.

Sparks, R.S.J., Marshall, L.A., 1986. Thermal and mechanical constraints on mixing between mafic and silicic magmas. Journal of Volcanology and Geothermal Research 29, 99–124.

Straub, S.M., LaGatta, A.B., Martin-Del Pozzo, A.L., Langmuir, C.H., 2008. Evidence from high-Ni olivines for a hybridized peridotite/pyroxenite source for orogenic andesites from the central Mexican Volcanic Belt. Geochemistry, Geophysics, Geosystems 9, Q03007.

Streck, M.J., Leeman, W.P., Chesley, J., 2007. High-magnesian andesite from Mount Shasta: a product of magma mixing and contamination, not a primitive mantle melt. Geology 35, 351–354.

Sun, S.S., McDonough, W., 1989. Chemical and isotopic systematics of oceanic basalts: implications for mantle composition and processes. Geological Society, London, Special Publications 42, 313–345.

Tamura, Y., Sato, T., Fujiwara, T., Kodaira, S., Nichols, A., 2016. Advent of continents: a new hypothesis. Scientific Reports 6, 33517.

Tatsumi, Y., 2001. Geochemical modeling of partial melting of subducting sediments and subsequent melt-mantle interaction: generation of high-Mg andesites in the Setouchi volcanic belt, southwest Japan. Geology 29, 323–326.

Tatsumi, Y., Suzuki, T., Kawabata, H., Sato, K., Miyazaki, T., Chang, Q., Takahashi, T., Tani, K., Shibata, T., Yoshikawa, M., 2006. The petrology and geochemistry of Oto-Zan composite lava flow on Shodo-Shima Island, SW Japan: remelting of a solidified high-Mg andesite magma. Journal of Petrology 47, 595–629.

Turner, S.J., Langmuir, C.H., 2015. The global chemical systematics of arc front stratovolcanoes: evaluating the role of crustal processes. Earth and Planetary Science Letters 422, 182–193.

Wang, Q., Wyman, D.A., Xu, J.F., Dong, Y.H., Vasconcelos, P.M., Pearson, N., Wan, Y.S., Dong, H., Li, C.F., Yu, Y.S., Zhu, T.X., Feng, X.T., Zhang, Q.Y., Zi, F., Chug, Z.Y., 2008a. Eocene melting of subducting continental crust and early uplifting of central Tibet: evidence from central-western Qiangtang high-K calc-alkaline andesites, dacites and rhyolites. Earth and Planetary Science Letters 272, 158–171.

Wang, Q., Wyman, D.A., Xu, J.F., Wan, Y.S., Li, C.F., Zi, F., Jiang, Z.Q., Qiu, H.N., Chu, Z.Y., Zhao, Z.H., Dong, Y.H., 2008b. Triassic Nb-enriched basalts, magnesian andesites, and adakites of the Qiangtang terrane (Central Tibet): evidence for metasomatism by slab-derived melts in the mantle wedge. Contributions to Mineralogy and Petrology 155, 473–490.

Wang, Q., Li, Z.X., Chung, S.L., Wyman, D.A., Sun, Y.L., Zhao, Z.H., Zhu, Y.T., Qiu, H.N., 2011. Late Triassic high-Mg andesite/dacite suites from northern Hohxil, North Tibet: geochronology, geochemical characteristics, petrogenetic processes and tectonic implications. Lithos 126, 54–67.

Weislogel, A.L., 2008. Tectonostratigraphic and geochronologic constraints on evolution of the northeast Paleotethys from the Songpan-Ganzi complex, central China. Tectonophysics 451, 331–345.

Wilson, M., 1989. Igneous Petrogenesis. Springer, Harper Collins Academic, London.

Wood, B.J., Turner, S.P., 2009. Origin of primitive high-Mg andesite: constraints from natural examples and experiments. Earth and Planetary Science Letters 283, 59–66.

Woodhead, J.D., Hergt, J.M., Davidson, J.P., Eggins, S.M., 2001. Hafnium isotope evidence for 'conservative' element mobility during subduction zone processes. Earth and Planetary Science Letters 192, 331–346.

Xiao, L., Zhang, H.F., Clemens, J.D., Wang, Q.W., Kan, Z.Z., Wang, K.M., Ni, P.Z., Liu, X.M., 2007. Late Triassic granitoids of the eastern margin of the Tibetan Plateau: geochronology, petrogenesis and implications for tectonic evolution. Lithos 96, 436–452.

Yin, A., Harrison, T.M., 2000. Geologic evolution of the Himalayan-Tibetan orogen. Annual Review of Earth and Planetary Sciences 28, 211–280.

Yuan, C., Zhou, M.F., Sun, M., Zhao, Y., Wilde, S., Long, X., Yan, D., 2010. Triassic granitoids in the eastern Songpan Ganzi Fold Belt, SW China: magmatic response to geodynamics of the deep lithosphere. Earth and Planetary Science Letters 290, 481–492.

Zhai, Q.G., Jahn, B.M., Su, L., Wang, J., Mo, X.X., Lee, H.Y., Wang, K.L., Tang, S.H., 2013. Triassic arc magmatism in the Qiangtang area, northern Tibet: zircon U–Pb ages, geochemical and Sr–Nd–Hf isotopic characteristics, and tectonic implications. Journal of Asian Earth Sciences 63, 162–178.

Zhang, H.F., Zhang, L., Harris, N., Jin, L.L., Yuan, H.L., 2006. U-Pb zircon ages, geochemical and isotopic compositions of granitoids in Songpan-Garze fold belt, eastern Tibetan Plateau: constraints on petrogenesis and tectonic evolution of the basement. Contributions to Mineralogy and Petrology 152, 75–88.

Zhang, H.F., Parrish, R., Zhang, L., Xu, W.-C., Yuan, H.-L., Gao, S., Crowley, Q.G., 2007. A-type granite and adakitic magmatism association in Songpan-Garze fold belt, eastern Tibetan Plateau: implication for lithospheric delamination. Lithos 97, 323–335.

Zhang, C.Z., Li, B., Cai, H.X., Tang, X.C., Wei, Q.G., Zhang, Y.X., 2008. A-type granite and adakitic magmatism association in Songpan-Garze fold belt, eastern Tibetan Plateau: implication for lithospheric delamination: comment. Lithos 103, 562–564.

Zhang, K.J., Li, B., Wei, Q.G., 2012. Diversified provenance of the Songpan-Ganzi Triassic turbidites, central China: constraints from geochemistry and Nd isotopes. The Journal of Geology 120, 69–82.

Zhang, L.Y., Ding, L., Pullen, A., Xu, Q., Liu, D.L., Cai, F.L., Yue, Y.H., Lai, Q.Z., Shi, R.D., Ducea, M.N., Kapp, P., Chapman, A., 2014. Age and geochemistry of western Hoh-Xil–Songpan-Ganzi granitoids, northern Tibet: implications for the Mesozoic closure of the Paleo-Tethys ocean. Lithos 190–191, 328–348.

Zhang, X.Z., Dong, Y.S., Wang, Q., Dan, W., Zhang, C.F., Deng, M.R., Xu, W., Xia, X.P., Zeng, J.P., Liang, H., 2016. Carboniferous and Permian evolutionary records for the Paleo-Tethys Ocean constrained by newly discovered Xiangtaohu ophiolites from central Qiangtang, central Tibet. Tectonics 35, 1670–1686.